Unimolecular Fragmentation Induced By Low Energy Collision: Statistically Or Dynamically Driven?

ARTICLE *in* THE JOURNAL OF PHYSICAL CHEMISTRY A · OCTOBER 2014

Impact Factor: 2.69 · DOI: 10.1021/jp5076059 · Source: PubMed

4 AUTHORS:

Ana Martin-Somer
CNRS
8 PUBLICATIONS **45** CITATIONS
SEE PROFILE

Manuel Yanez
Universidad Autónoma de Madrid
271 PUBLICATIONS **3,747** CITATIONS
SEE PROFILE

Marie-Pierre Gaigeot
Université d'Évry-Val-d'Essonne
104 PUBLICATIONS **1,817** CITATIONS
SEE PROFILE

Riccardo Spezia
Université d'Évry-Val-d'Essonne
109 PUBLICATIONS **1,059** CITATIONS
SEE PROFILE

THE JOURNAL OF PHYSICAL CHEMISTRY A

Article

pubs.acs.org/JPCA

Unimolecular Fragmentation Induced By Low-Energy Collision: Statistically or Dynamically Driven?

Ana Martín-Sómer,[†,‡] Manuel Yáñez,*[,†] Marie-Pierre Gaigeot,[‡,§,∥] and Riccardo Spezia*[,‡,§]

[†]Departamento de Química, Facultad de Ciencias, Módulo 13. Universidad Autónoma de Madrid, Campus de Excelencia UAM-CSIC. Cantoblanco, E-28049 Madrid, Spain

[‡]Université d'Evry Val d'Essonne, UMR 8587 LAMBE, Boulevard F. Mitterrand, 91025 Evry Cedex, France

[§]CNRS, Laboratoire Analyse et Modélisation pour la Biologie et l'Environnement, UMR 8587, Boulevard F. Mitterrand, 91025 Evry Cedex, France

[∥]Institut Universitaire de France (IUF), 103 Blvd St Michel, 75005 Paris, France

Supporting Information

ABSTRACT: By combining chemical dynamics simulations and RRKM statistical theory we have characterized collision induced dissociation (CID) mechanisms of $[M(formamide)]^{2+}$ ions (M = Ca, Sr) at different timescales, from few femtoseconds to microseconds. Chemical dynamics simulations account for the short-time and dynamically driven reactivity, such as impulsive collision mechanism for formamide neutral loss. From the simulations, we also got the amounts of energy transferred during the collision and, especially important, the vibrational and rotational energy distributions of the ions that did not react during the simulation time length of 2.5 ps. These internal energy distributions were in turn used in combination with RRKM theory to estimate the rate constants of the possible reactive pathways. Hence, we performed a statistical analysis of the CID dynamics accounting for the long-time and statistical reactivity (i.e., through an IVR mechanism). This multiscale approach allowed us to account for all the products observed in the CID experimental spectra of $[Ca(formamide)]^{2+}$ and $[Sr(formamide)]^{2+}$ doubly charged cations, as well as the differences between them.

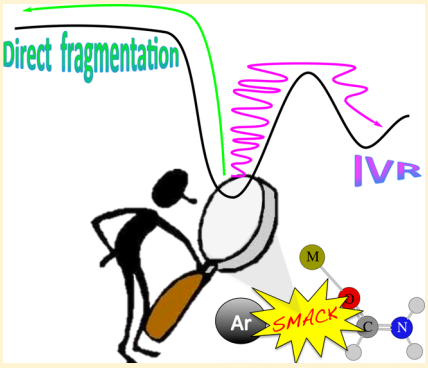

1. INTRODUCTION

The simplest chemical reactions are gas phase unimolecular events. These events are associated with fragmentation reactions, and though they are simple, the physical-chemistry processes involved can be quite complex (e.g., geometrical and electronic rearrangements, direct fragmentation, or fragmentation after energy distribution within the molecule). Unimolecular reactions are related with many important phenomena occurring in the gas phase and understanding the fundamentals of these reactions provides important knowledge for the structural, energetic, and reactivity properties of the molecule under study.

Different techniques can be used for activating ions, which differ by the energy range employed, the instrument, and the activation mechanisms.[1−3] Notable among them is collision-induced dissociation (CID), where the ion is made to collide with an inert gas at low collision energies, in such a way that part of the kinetic energy is transferred to the molecular ion as vibrational and rotational internal energy. CID has been extensively used to study ion structure and is one of the most common ion activation methods.[2,4−10] Nevertheless, there are many details of gas-phase dissociation mechanisms associated with CID that are still unclear. In this realm, theoretical calculations can help to understand the CID processes and in particular provide an atomistic description of the mechanisms and pathways leading to the final fragments. Statistical models such as transition state theory (TST) and Rice-Ramsperger-Kassel-Marcus (RRKM) theory[11−18] have been (and are) extensively used to describe the kinetics of the unimolecular fragmentation induced by collisions.[2,3,15,19−23] However, evidence of nonstatistical dynamics, or non-RRKM, in CID has been reported both in experiments[24,25] and simulations,[26−30] as well as the importance of impulsive collision mechanisms to understand CID in protonated amino acids and peptides.[31,32] One mechanism, identified as "shattering",[33−35] occurs in surface-induced dissociation (SID),[36−39] where the projectile ion fragments as it collides with the surface. In CID a similar mechanism, where the bond breaks in one or less vibrational periods after collision, was proposed for a series of examples.[24−29] This often corresponds to an impulsive (i.e., spatially localized) model of the collisional energy transfer mechanism, while RRKM theory uses the assumption that the collision completely delocalizes the reactant molecule on the final state energy surface.[40]

Two limiting fragmentation mechanisms can be described to explain CID reactivity. One in which the collision locally

Received: July 28, 2014
Revised: October 10, 2014
Published: October 21, 2014

   dx.doi.org/10.1021/jp5076059 | J. Phys. Chem. A 2014, 118, 10882−10893

activates one (or few) vibrational mode(s), and the fragmentation occurs within one vibrational period before intramolecular vibrational energy redistribution (IVR) could take place. We will call here, and hereafter, this mechanism, that implies an impulsive collision energy transfer, direct fragmentation.[41] In the second mechanism, the translational energy transferred to the molecule is redistributed among its vibrational and rotational modes. If the energy in a vibrational mode is higher than the energy required for breaking this bond, the molecule eventually dissociates. Reactions taking place via the latter mechanism can be accounted for through statistical theories such as RRKM, while in the case of the first mechanism, a pure dynamical picture where the reaction is faster than IVR, the reactivity can only be understood by means of dynamics simulations. Therefore, an important question concerning CID unimolecular reactivity is whether the mechanisms leading to the different fragmentation pathways are statistical or not.

Particularly interesting is the CID of doubly charged cations because, in addition to the neutral loss reactive pathway observed in monocharged species, they can fragment as well via Coulomb explosion mechanisms. This is a fragmentation mechanism resulting from an internal molecular arrangement ending in two single charges on the same molecule that then explodes due to electrostatic repulsion, yielding two single-charged fragments. Thus, it is also possible to study the competition between both reactive pathways. Additionally, doubly charged molecular ions are of great importance in chemical and biochemical processes, both in solution and in the gas phase.[42] In spite of their short lifetime, they are fundamental in gas-phase ion chemistry and in mass spectrometry.[43−45] They also play important roles in photochemical processes,[46,47] as well as in astrochemistry and the chemistry of the atmosphere.[48−51] It was also reported that they may have played some role in the origin of life,[52−56] inducing the precipitation of nucleic acid molecules. On top of that, due to the absence of solute−solvent or solute−counterion interactions, it is possible to understand the intrinsic physical-chemical properties of these molecular ions. We have recently studied the statistical kinetics of $[Ca(formamide)]^{2+}$ and $[Sr(formamide)]^{2+}$ dications,[57] complementing the previous investigations based only on the topology of the PESs.[58,59] However, there are still unanswered questions. Both molecules display a potential energy surface quite similar, while the experimental CID spectra for M = Ca shows the presence of Coulomb explosions fragmentation pathways nonexistent when M = Sr. Some other features of the CID spectra, as the presence of a very intense peak corresponding to the bare metal dication, M^{2+}, cannot be accounted for based solely on the topology of the PES, since this fragmentation corresponds to the most endothermic exit channel. Another shortcoming of using RRKM theory to model CID fragmentation is the fact that quite often only products corresponding to masses observed in CID experiments are considered.

Thus, the purpose of this study is two-fold: on the one hand to investigate and characterize the fragmentation mechanisms on CID experiments and, at the same time, provide an explanation to the differences observed in the CID spectra of $[Ca(formamide)]^{2+}$ and $[Sr(formamide)]^{2+}$ dications. With this aim, we compare the results of chemical dynamics simulations with the predictions obtained using RRKM statistical theory (short-time regime). Furthermore, by coupling the vibrational and rotational energy distributions obtained from chemical dynamics simulations of nonreactive trajectories with RRKM rate constants, $k(E)$, it is possible to model reactivity on the long-time scale, an important issue that is difficult to directly obtain only from chemical dynamics simulations. Thus, the combination of both methods provides a multiscale approach, allowing one to bridge the gap between the different timescales involved in CID experiments: short-time nonstatistical reactivity together with the long-time statistical reactivity.

2. COMPUTATIONAL DETAILS

2.1. Direct Dynamics Simulations. We performed direct dynamics simulations to model the CID process between Ar and $[M(formamide)]^{2+}$ (M = Ca, Sr) molecular ions. The total potential energy is

$$V = V_{ion} + V_{Ar-ion} \quad (1)$$

where V_{ion} and $V_{Ar\text{-}ion}$ are the ion intramolecular and the Ar-$[M(formamide)]^{2+}$ interaction potentials, respectively. A QM description is used to treat the intramolecular ion potential (V_{ion}), while the ion-projectile intermolecular interaction ($V_{Ar\text{-}ion}$) is treated via the analytical potential developed by Meroueh and Hase to simulate CID of protonated peptides.[60] This potential is a sum of two-body terms between Ar and each of the atoms of the molecular ion:

$$V_{Ar-ion} = \sum_i a_i \exp(-b_i r) + \frac{c_i}{r^9} \quad (2)$$

where r is the Ar/ion-atom distance and the a, b, and c coefficients are obtained by fitting the analytic potential to the ab initio interaction potential. The values for parameters a, b, and c for the Ar-formamide and $Ar-Ca^{2+}$ interactions were taken from refs 60 and 30. Parameters for the $Ar-Sr^{2+}$ interaction were found by fitting eq 2 to the $Ar-Sr^{2+}$ potential energy curve obtained at the QCISD(T)(full) level, together with a 6-31++G(d,p) basis set expansion for Ar atom and a Stuttgart basis set with pseudo potential for Sr^{2+} cation.[61] BSSE was taken into account using the counterpoise method.[62] The ab initio and fitted curves, as well as a, b, and c parameters are shown in Figure S1 of the Supporting Information. Note that the curve is fitted with a purely repulsive energy function in order to better describe the repulsive wall that is the most important feature in CID for the energies considered here.[60]

The molecule's nuclei positions, q_i and momenta p_i, evolve on the Born−Oppenheimer potential energy surface obtained by solving the time-independent Schrödinger equation at each configuration. For this purpose and based on our previous assessment work,[57] we used the G96LYP[63,64] and BLYP[63,65] functionals with the 6-31G(d) basis set for M = Ca and the G96LYP functional with 6-31G(d) basis set for one set of trajectories and 6-31+G(d,p) for the other set for M = Sr.

In our approach, we just modeled a single collision, which is a good approximation when the gas pressure is very low. For the initial conditions, we used the minimum energy structure (min**1**) of $[M(formamide)]^{2+}$ (M = Ca, Sr) (see Figure 1).

Since the electrospray ionization source used in the CID experiments is not thermalized, we chose an initial temperature of 300 K for the ions as is usually done in similar studies.[30,31,60,66−68] Energies for the normal modes of vibration were selected from a 300 K Boltzmann distribution. The resulting normal modes energies were partitioned between kinetic and potential energy by choosing a random phase for

dx.doi.org/10.1021/jp5076059 | J. Phys. Chem. A 2014, 118, 10882−10893

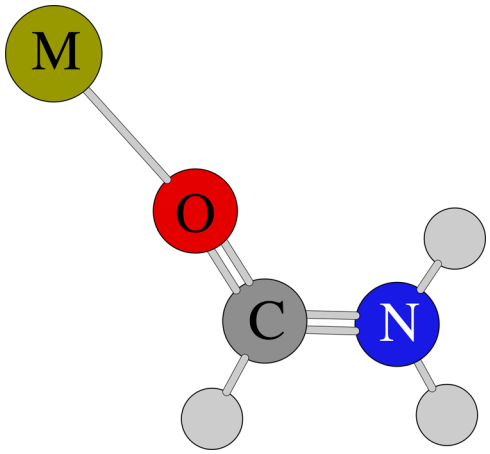

Figure 1. Global energy minimum (min**1**) of $[M(formamide)]^{2+}$ (M = Ca, Sr). This structure is used to select the initial conditions for the dynamics simulations.

each normal mode. Rotational energy and angular momentum for the polyatomic molecule were selected by assuming separability of vibrational and rotational motion. Thus, initial rotational conditions are obtained by assuming a thermal partitioning of RT/2 about each internal rotational axis. Afterward, vibrational and rotational energies are transformed into Cartesian coordinates and momenta following algorithms implemented in VENUS.[69,70] Random orientations in Euler angles between the (rigid body) ion and projectile (Ar atom) are sampled in order to account for the random directions of the Ar − $[M(formamide)]^{2+}$ collisions. Then the ion-projectile relative energy is set and possible impact parameters are considered. The impact parameter (b) is sampled between zero and b_{max} = 3.0 Å. Finally, the collision is done at a given energy defined in the center-of-mass of the system composed by the ion and the projectile, E_{CM}, that is in relation with the laboratory framework energy, E_{LAB} (directly set in the instrument):

$$E_{CM} = \frac{m_2}{m_1 + m_2} E_{LAB} \tag{3}$$

where m_1 and m_2 are the masses of the ion and the projectile, respectively. A detailed review of collision dynamics as in CID is reported by Douglas.[71] We considered three center-of-mass collision energies: 180, 230, and 280 kcal mol^{-1}, which match the experimental energy range of the available experiments.[58,59]

The trajectories were calculated using VENUS[69,70] coupled to Gaussian09.[72] The classical equations of motion were integrated using the velocity Verlet algorithm[73] with a time step of 0.2 fs that gives energy conservation for both reactive and nonreactive trajectories. The initial ion−Ar distance is 8.0 Å, and the trajectories are stopped at a 100 Å ion−Ar distance. This corresponds to a total integration time of about 2.5 ps per trajectory. A trajectory was also stopped if a reactive channel was identified. In that case, a criterion distance of 7.0 Å was used to guarantee no interactions between fragments. For each case, 300 trajectories were computed to correctly describe the process under study.[74]

To deepen the analysis of the CID fragmentation mechanisms, we computed the NBO charges for a trajectory yielding neutral loss and a trajectory yielding Coulomb explosion. The NBO analysis has been carried out with NBO-5.0.[75]

2.2. RRKM Rate Constants. The RRKM rate constants were obtained from a previous study on the fragmentation kinetics of $[M(formamide)]^{2+}$ ions (M = Ca, Sr).[57] In this study, we used RRKM statistical theory in order to compute quantum harmonic microcanonical rate constants, $k(E)$ (i.e., taking into account the zero-point vibrational energy and using harmonic frequencies). In its simplest formulation, where rotations are ignored and TS location is assumed to be fixed at a saddle point (tight-TS), the expression describing the internal energy-dependent rate constant for a fragmentation reaction is

$$k(E) = \frac{\sigma}{h} \frac{N^{\ddagger}(E - E_0)}{\rho(E)} \tag{4}$$

where σ is the reaction degeneracy, E_0 is the threshold energy, $N^{\ddagger}(E - E_0)$ is the TS sum of states, and $\rho(E)$ is the reactant density of states. The latter two quantities are only for active degrees of freedom. Normally, the modes treated as active are all the normal modes. External rotation can also be considered when computing the rate constant if the external rotational degrees of freedom are added to the modes treated as active. There are different ways of doing so in the framework of RRKM theory.[76] For the rate constants computed in this work, we assumed that the molecule (min**1**, see Figure 1) can be considered an almost symmetric top, where $I_x \approx I_y$ and with rotational energy given by the following approximation:[77]

$$E_{rot}(J, K) = \left(\frac{1}{I_x} + \frac{1}{I_y}\right)\frac{[J(J+1) - K^2]\hbar^2}{4} + \frac{K^2\hbar^2}{2I_z} \tag{5}$$

The symmetry axis is the z axis and the other two moments of inertia are $I_x \approx I_y$. For the $k(E)$ shown here, J and K quantum numbers were treated adiabatically (no energy exchange between vibrational and rotational modes is allowed), and the rotational energy is equally distributed among the three axes [$E_{rot}(x,y) = 2/3E_{rot,tot}$ and $E_{rot}(z) = 1/3E_{rot,tot}$], since the molecule is an almost symmetric top). Within this assumption (J and K adiabatic), the RRKM unimolecular rate constant for energy E and specific values of J and K is given by[15]

$$k(E, J, K) = \frac{\sigma}{h} \frac{N^{\ddagger}[E - E_0 - E^{\ddagger}_{rot}(J, K)]}{\rho[E - E_{rot}(J, K)]} \tag{6}$$

where $E^{\ddagger}_{rot}$ is the rotational energy for the transition state and E_{rot} is the same for the minimum energy structure (both obtained using eq 5). Further details on how we computed the rate constants, and in particular how rotational energy was taken into account, are given in ref 57. For additional information, the reader is referred to the extensive literature on RRKM theory.[12−18]

Thus, using RRKM theory, the rate constants are computed by using properties of minima and saddle points on the PES and the internal energies that are obtained from nonreactive chemical dynamics simulations. The basic assumptions are that a microcanonical ensemble is maintained as the molecule dissociates, that the rate constant depends only on the total energy E and the total angular momentum J and does not depend upon where the energy is initially located. This is equivalent to assume that IVR is rapid compared to the rate of reaction/isomerization.[15]

3. RESULTS

3.1. Dynamical Reaction Products. The main processes after the collision with Ar are (i) conversion of collisional

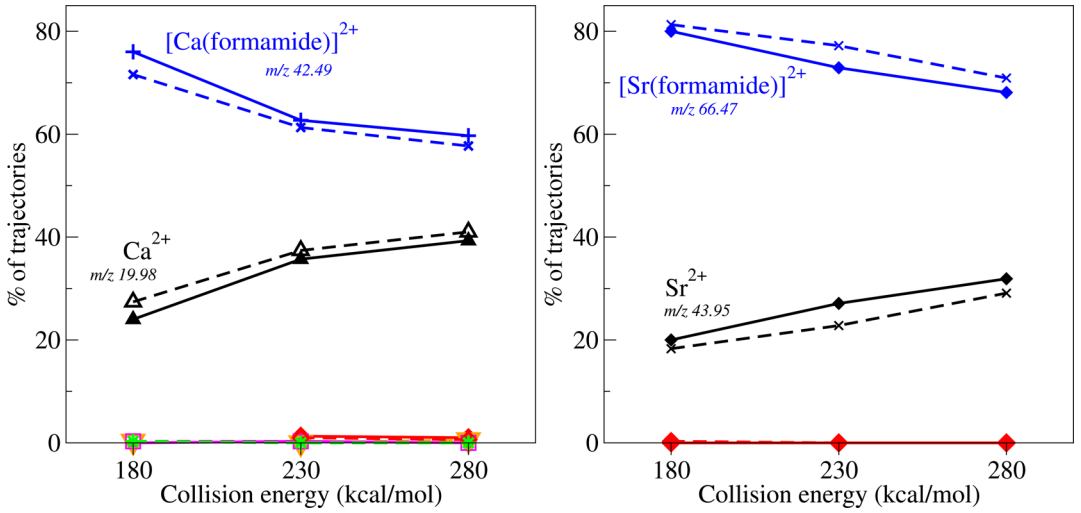

Figure 2. Percentages of trajectories for each channel as a function of the collision energy. Nonreactive trajectories (blue); product M^{2+} + formamide (black). For details on products observed in less than 2%, reported in green (an intermediate structure called int**10** (see Scheme 1b), red ($[M(NH_2)^+ + HCO^+]$), and magenta ($[Ca(NH_3)]^{2+}$) (see Table 1). The simulations were performed at two levels of theory: for M = Ca (left) G96LYP/6-31G(d) (solid lines) and BLYP/6-31G(d) (dashed lines). For M = Sr (right) G96LYP/6-31G(d) (solid lines) and G96LYP/6-31+G(d,p) (dashed lines).

Table 1. Products Ratio Obtained from Chemical Dynamics Simulations Starting in the Global Minimum, min1, for M = Ca (top) and M = Sr (bottom)

$[Ca(formamide)]^{2+}$						
	G96LYP/6-31G(d)			BLYP/6-31G(d)		
collision energy	180	230	280	180	230	280
non reactive	76.0%	62.7%	59.7%	71.6%	61.3%	57.7%
Ca^{2+} + formamide	24.0%	35.7%	39.3%	27.4%	37.4%	41.0%
$[Ca(NH_2)]^+ + [HCO]^+$	–	1.3%	1.0%	–	1.0%	0.6%
$[Ca(NH_3)]^{2+}$ + CO	–	0.3%	–	0.3%	0.3%	–
int**10**	–	–	–	0.3%	–	–
$[Sr(formamide)]^{2+}$						
	G96LYP/6-31G(d)			G96LYP/6-31+G(d,p)		
collision energy	180	230	280	180	230	280
nonreactive	80.0%	72.9%	68.1%	81.3%	77.2%	70.9%
Sr^{2+} + formamide	20.0%	27.1%	31.9%	18.3%	22.8%	29.1%
$[Sr(NH_2)]^+ + [HCO]^+$	–	–	–	0.3%	–	–

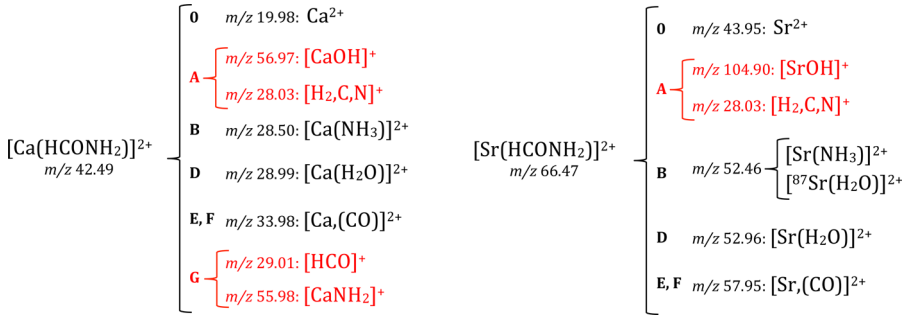

Figure 3. Masses observed in the experimental CID spectrum of $[M(formamide)]^{2+}$ together with their molecular formulas. M = Ca (left), M = Sr (right). In black are neutral losses and in red Coulomb explosions. Data taken from ref 59 and 58, respectively.

energy into internal energy of scattered ions; (ii) sequential activation of a bond and reactivity observed in the simulation time length (2.5 ps); and (iii) direct fragmentation after the collision (for example, an atom is knocked out). Figure 2 summarizes the products obtained during the 2.5 ps simulations. The product ratios are given in Table 1.

The results do not significantly differ from one method to another. The first conspicuous fact is that the reactivity is not very high (<40% of the trajectories react), and it is larger for calcium than for strontium. In the time length of our simulations (~2.5 ps maximum) both kinds of reactive channels, neutral losses and Coulomb explosions, are observed.

dx.doi.org/10.1021/jp5076059 | J. Phys. Chem. A 2014, 118, 10882−10893

The former corresponds to the loss of formamide and CO yielding as accompanying ions M^{2+} and $[Ca(NH_3)]^{2+}$, respectively, and the latter to the fragmentation into $[M(NH_2)]^+ + [HCO]^+$. Note that the loss of CO is only observed for M = Ca.

These results are in good agreement with CID experimental spectra (see Figure 3).[58,59] Most of the trajectories did not react, which agrees with the fact that the peak for the parent ion is the most intense. Among the reactive ones, the vast majority undergoes formamide neutral loss, the second most intense peak in the experiment. Similarly, neither the loss of CO nor the ions corresponding to the **G** Coulomb explosion are observed in the formamide-Sr^{2+} reactions, in agreement with our simulations. Indeed, no trajectories end in products **B** when M = Sr and only 0.3% of the trajectories follow the **G** Coulomb explosion pathway. It is worth noting however that some other products, which appear in the experimental spectra, did not show up in our chemical dynamics simulations, likely because the simulation time (2.5 ps) was too short. Note that some products are observed with very low percentage (0.3−1.3%) that, given the relative low number of DFT-based trajectories, correspond to a few trajectories (1−4). Of course, the uncertainty associated is relatively high, such that the appearance of these products should be considered here just as the possibility of obtaining them and not quantitatively. Furthermore, it should be noticed that under the experimental conditions, the ions might undergo multiple collisions while with direct dynamics trajectories, we only model reactivity due to a single collision.

3.2. Effects of the Collision Energy on the Reactivity. The agreement between our simulations and the experiments is also good as far as the effects of the collision energy on the reactivity are concerned. Indeed, our theoretical results show that for all collision energies, formamide neutral loss (O−M bond dissociation) clearly prevails over the other fragmentation pathways (which are observed for less than 1.5% of the trajectories), increasing almost linearly with the collision energy (see Figure 2). This is consistent with an impulsive collision mechanism occurring for this reactive channel (vide infra). For the **G** Coulomb explosion channel, giving rise to an HCO^+ peak, the maximum number of trajectories following this path is observed for 230 kcal mol^{-1} collision energy, while it does not appear for the lowest collision energy used in the simulations (180 kcal mol^{-1}). On the contrary, the **B** exit channel is not observed at the highest energy, while it appears at low (BLYP) and middle energies (BLYP and G96LYP). Int**10**, that appears for 180 kcal mol^{-1} collision energy (BLYP), is an intermediate structure between min**1** and product **B** that will eventually evolve to product **B** (see Scheme 1). The different effects of the collision energy on each reactive channel are better understood when considering the mechanisms for each pathway, as will be discussed in the following section.

3.3. Reaction Mechanisms. An important feature of the chemical dynamics simulations is that they provide an atomic-level description of the fragmentation mechanisms. There are three main ways in which the collision between the Ar and the molecular ion takes place providing subsequent reactivity (Figure 4): (i) Ar hits the metal more or less perpendicularly to the M−O−C bond, (ii) Ar strikes the formamide molecule on the C═O bond and perpendicularly to the molecular plane, or (iii) the collision takes place on the NH_2 group side, and its rotation is thus activated.

Scheme 1. Kinetic Scheme for the Reactions That Can Take Place Starting from the Intermediates int2 and int10 for Both $[Ca(formamide)]^{2+}$ and $[Sr(formamide)]^{2+}$

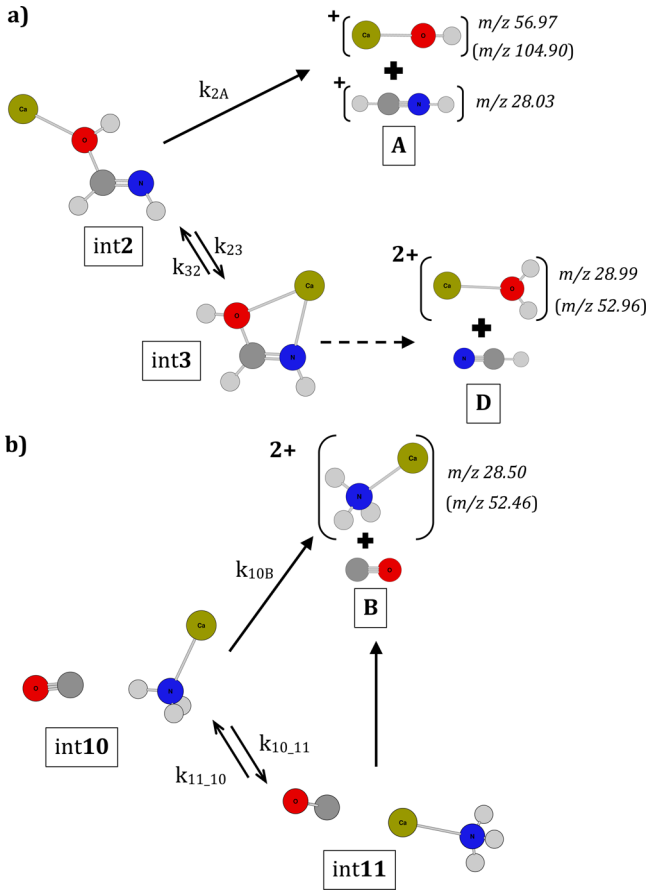

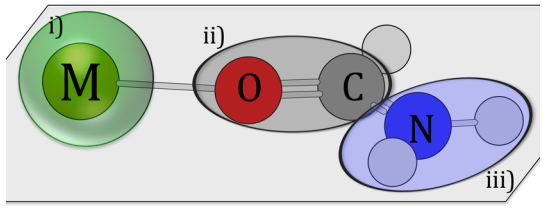

Figure 4. Different possibilities for the collision between Ar and the molecular ion providing subsequent dissociation, observed in our chemical dynamics simulations.

The vast majority of trajectories result in formamide neutral loss, regardless of the collision site. When Ar hits calcium perpendicular with respect to the M−O−C bond (i), the collision drives the metal away from formamide (see movie jp5076059_si_002). This mechanism is similar to the "golf like" mechanism found by Spezia et al.[30] for CID of $[Ca(urea)]^{2+}$. When the collision is perpendicular to the C═O bond (ii), M^{2+} also detaches from formamide, breaking the M−O bond (see movie jp5076059_si_003). Also, the M−O easily breaks for the collisions at the NH_2 group, when enough energy is transferred to the ion (see movie jp5076059_si_004). Still, there is a difference due to the metal in the complex. In the case of Ca, more than one-third of the reactive trajectories directly strip off the metal, whereas for Sr, which is more than twice heavier than Ca, the number of these trajectories is much smaller. In a similar way, neutral loss of formamide in the

dx.doi.org/10.1021/jp5076059 | J. Phys. Chem. A 2014, 118, 10882−10893

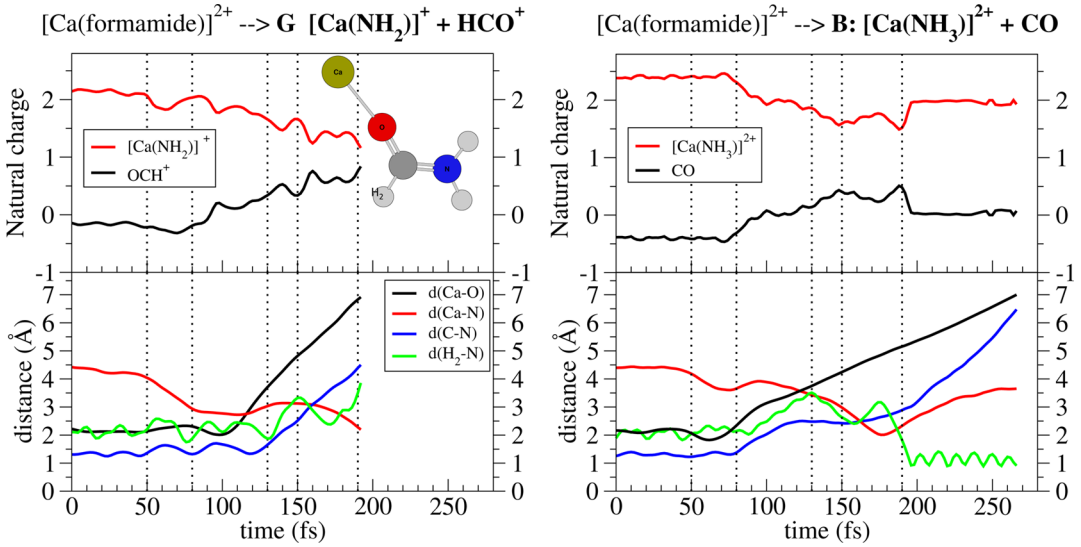

Figure 5. Evolution with time of natural charge (top panel) and distances (bottom panel) for a trajectory yielding **G**: $[Ca(NH_2)]^+ + HCO^+$ Coulomb explosion (left) and **B**: $[Ca(NH_3)]^{2+} + CO$ neutral loss (right).

$[M(formamide)]^{2+}$ systems studied here can be classified as "impulsive collision" mechanisms, as the M−O bond breaks just after the Ar collision on the same M−O bond. Therefore, the probability of breaking the M−O bond increases with the collision energy.

When the collision takes place at the NH_2 group (iii), products **G** (Coulomb explosion), **B** (neutral loss), as well as the formation of int**10** are also observed. The mechanism to arrive to **G** and **B** is very similar, with only very subtle differences between the two. In Figure 5, the evolution of the natural charge with time for the two final fragments is plotted, as well as some representative distances, for one trajectory yielding **G** ($[Ca(NH_2)]^+ + HCO^+$) and another yielding **B** ($[Ca(NH_3)]^{2+} + CO$).

In both processes, the first 50 fs correspond to the approaching of Ar toward the molecular dication. After the collision in process **G**, the first significant change is a decrease of the COCa angle, which brings the metal closer to the amino group such that, after 100 fs, the Ca−N bond is practically formed and at that time both the Ca−O and the C−N bond start cleaving in an almost synchronous way. This leads to $[CaNH_2]^+$ and $[HCO]^+$ fragments, which repel each other as shown by the steep increase of both Ca−O and C−N distances. Coherently, the net charges of the two fragments also start to change significantly at ca. 100 fs. Conversely, for process **B**, the first effect of the collision is the almost synchronous cleavage of Ca−O and C−N bonds, so that after 100 fs, Ca−O and Ca−N distances become very similar, indicating that the metal is bridging between the HCO and NH_2 groups. The separation of both subunits is not taking place until later. This allows the HCO group to reorient itself in order to favor a proton transfer toward the $CaNH_2$ moiety at around 200 fs, reflected by the sudden decrease of the N−H distance (light-green line). Thus, for low-collision energies, there are more probabilities for obtaining **B**, since the relative movement of the two subunits will be slow, facilitating the aforementioned proton transfer, whereas at high collision energies, the Coulomb explosion should be greatly favored. The movies for both trajectories can be found in the Supporting Information (movies jp5076059_si_005 and and jp5076059_si_006).

Figure 6 shows the simulation times (in fs) for chemical reactivity for all the trajectories. It is apparent that formamide neutral loss reaction covers a long time-span, from a few femtoseconds up to ∼1.7 ps, whereas the other reactions observed (**G** Coulomb explosion and CO neutral loss, **B**) are always fast, taking place in less than 1 ps. Looking into the details of each trajectory, we observe that the fast (<1 ps) formamide neutral loss reactions occur, thanks to an impulsive collision energy transfer mechanism, in which the energy is deposited into the M^{2+} + formamide relative motion leading to direct dissociation before one Ca−O vibrational period, thus following the direct fragmentation mechanism described in Introduction. However, this is not the case for the remaining reactions, namely, "slow" formamide neutral loss, **G** Coulomb explosion, and CO neutral loss, **B**. In these instances, there are some molecular rearrangements and/or energy distribution within the internal modes of the molecule. However, does a complete IVR, as assumed in RRKM theory, occur? To answer this question, we plotted in Figure 7 the reaction times as a function of the internal energy for each trajectory yielding Ca^{2+} (left) and **G** Coulomb explosion (right), together with the half-life times ($t_{1/2}$) predicted from RRKM rate constants as a function of the internal energy of the molecule. The corresponding graphs for formamide neutral loss at the BLYP/6-31G(d) level, as well as for Sr^{2+} at G96LYP/6-31G(d) and G96LYP/6-31+G(d,p) are shown in Figures S2 and S3 of the Supporting Information, respectively.

There are only two points on the figure on the right (k_{1G}) that match with the predicted RRKM reaction times. However, in general, both sets of times differ significantly, indicating that the trajectories which do not follow a direct fragmentation mechanism neither react through a full IVR mechanism, which is assumed in the RRKM theory. This suggests that the actual mechanism is in between these two limiting cases (i.e., the energy is distributed within the internal degrees of freedom of the molecule), but the reaction takes place before a complete IVR could be achieved. Thus, we called this mechanism energy transfer, ET, as already proposed by Spezia et al.[67] These reactions are slower than if they followed direct fragmentation mechanism reactions, but they are still faster than predicted by RRKM theory (complete IVR mechanism). In Figure S4 of the

dx.doi.org/10.1021/jp5076059 | J. Phys. Chem. A 2014, 118, 10882−10893

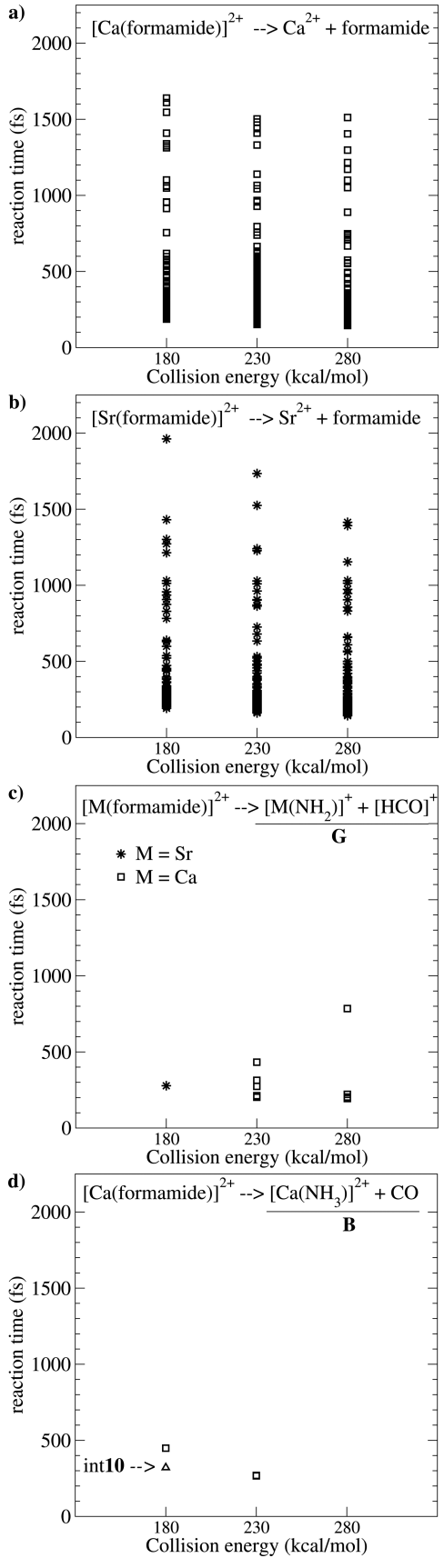

Figure 6. Simulation times (fs) for the reactive trajectories at the different collision energies: 180, 230, and 280 kcal mol^{-1}. Each point represents one trajectory. Squares are for M = Ca and stars for M = Sr.

Supporting Information, we show an example of how bonding vibrations are affected by the collision with Ar. As specified in the Supporting Information, during the collision and at the time of the reaction, the molecular vibrations cannot be attributed to one specific reference structure and to any ro-vibrational modes. Thus, only qualitative considerations can be done on how internal modes are activated at the time of the reaction (for example, the C═O distance increases largely from initial one when Ar is colliding and then it decreases to a distance corresponding to products). For the sake of simplicity, we used as a prototypical example the reaction leading to **G** products (the same trajectory shown in Figure 5a and reported in the movie jp5076059_si_005.mpg of the Supporting Information).

3.4. Nonreactive Trajectories. Another piece of information that can be extracted from our chemical dynamics simulations is the amount of energy that has been transferred during the collision to the molecular ion, shown in Figures S5 and S6 of the Supporting Information. Much more important, however, is to know how this energy is distributed after collision among the vibrational and rotational degrees of freedom for the initial ion (min**1**, see Figure 1) population that has not reacted in the 2.5 ps simulated by chemical dynamics. Figure 8 shows the vibrational (a panels) and rotational (b panels) energy distributions for both Ca and Sr containing molecular ions, computed at the G96LYP/6-31G(d) level of theory. Similar results (Figure S7 of the Supporting Information) were found with the other levels of theory.

We should note that the vibrational activation for the molecules that did not react is very important, reaching values up to 120 kcal mol^{-1}. One striking feature is that the energy found in the rotational degrees of freedom is also very high with values up to 80 kcal mol^{-1}. Hence, despite the fact that rotational activation is rarely considered in RRKM models applied to CID reactivity,[78−81] and in agreement with previous simulations of collisional activation of peptides,[66] planar Al clusters,[82] and molecular ions such as [Ca(urea)]$^{2+}$ colliding with Ar,[30] and protonated urea colliding with Ar[67] and N_2,[68] both vibrational and rotational excitations play a role in the process, being slightly larger for [Ca(formamide)]$^{2+}$ ions than for the Sr analogue. Due to the different masses, for Ca most of the ions have vibrational energies in the 10−20 kcal mol^{-1} interval while for Sr they are mainly in the 0−10 kcal mol^{-1} interval. In both cases, the population decreases sharply as the energy increases. The same patterns are found for the rotational excitation of both ions, having most of the ions at a rotational energy within the 0−10 kcal mol^{-1} range.

More importantly, for Ca, there is a fraction of the nonreactive molecules with enough vibrational energy to cross the barriers between min**1** and the five accessible TSs (showed as dashed vertical lines in Figure 8). Since the vibrational excitation is lower for Sr, only the lowest lying TSs can be reached. This suggests that **G** products are not observed in the CID experimental spectrum of [Sr(formamide)]$^{2+}$ (in contrast to what is found for [Ca(formamide)]$^{2+}$ ions) due to the lack of energy to reach the corresponding TSs.

Assuming that with enough time there will be a complete IVR, we can now couple the aforementioned chemical dynamics simulations with RRKM theory to build up a multiscale approach that assesses longer timescales. This coupling is simplified by the fact that vibrational excitation is independent of the rotational excitation (see Figures S8 and S9 of the Supporting Information).

dx.doi.org/10.1021/jp5076059 | J. Phys. Chem. A 2014, 118, 10882−10893

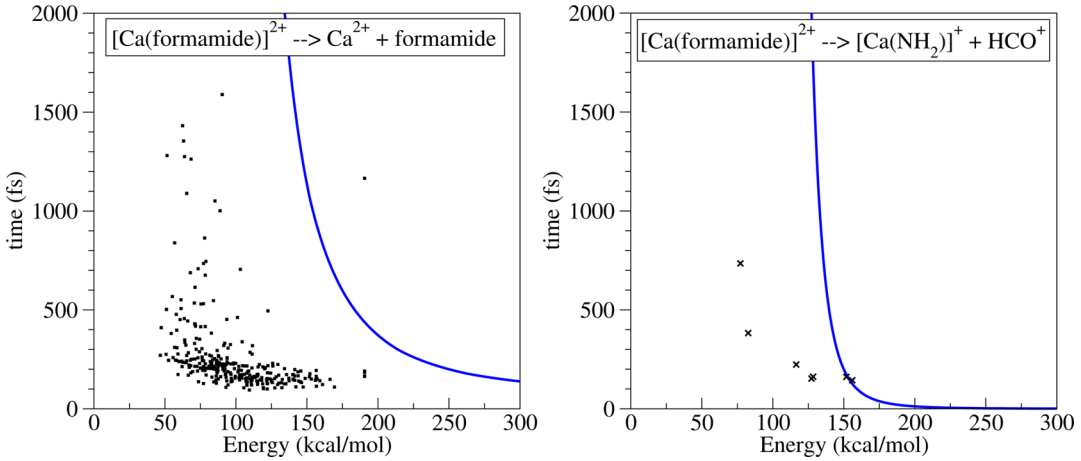

Figure 7. Reaction time vs energy transfer obtained from chemical dynamics simulations (■) and half-life times ($t_{1/2}$) predicted by RRKM (solid lines). Both were obtained using the G96LYP/6-31G(d) level of theory. Results are shown for trajectories yielding formamide neutral loss, k_{01} (left), and **G** Coulomb explosion, k_{1G} (right).

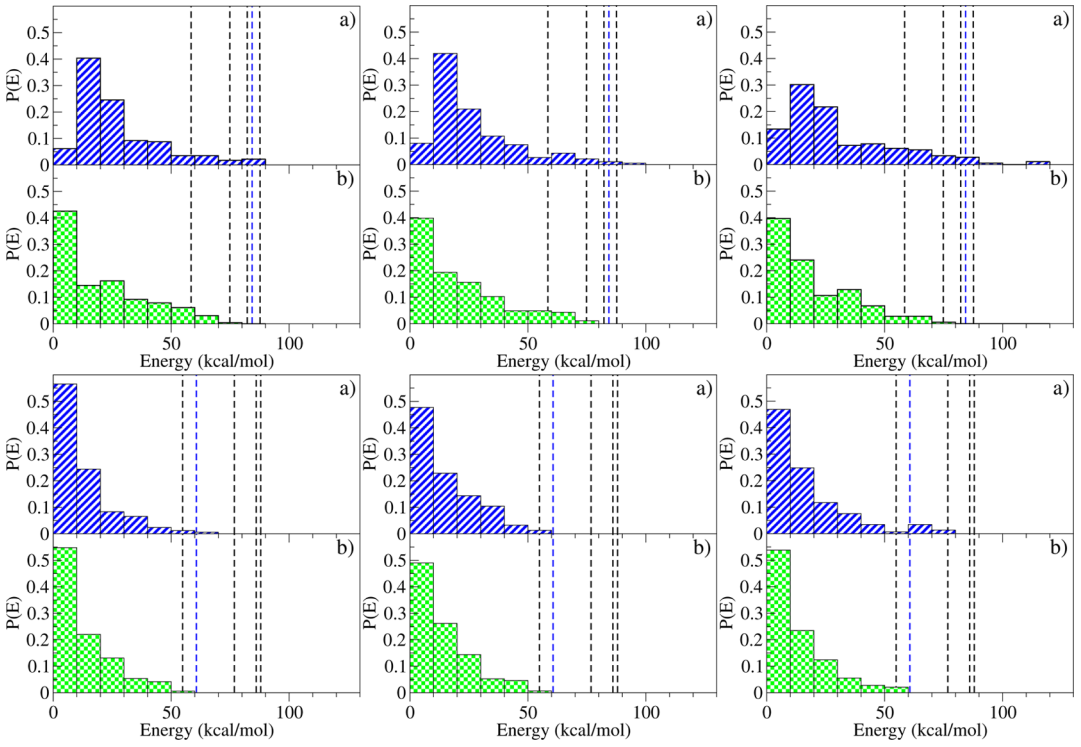

Figure 8. Vibrational (a panels) and rotational (b panels) energy distribution for the nonreactive trajectories at the three collision energies: 180, 230, and 280 kcal mol^{-1} from left to right. The three upper graphs correspond to M = Ca, while the three bottom ones are for M = Sr. Dashed vertical lines mark the energy for the different TS that can be reached from min**1** structure. All the values are computed at the G96LYP/6-31G(d) level of theory.

The upper part of Figure 9 shows the kinetic scheme for the reactions that can take place starting from min**1**, namely three isomerization reactions: min**1** → int**2** (k_{12}); min**1**→ int**5** (k_{15}); and min**1**→ int**10** (k_{110}); and two fragmentation channels: formamide neutral loss (k_{01}) and **G** Coulomb explosion (k_{1G}). The bottom part of Figure 9 shows the corresponding RRKM rate constants (black lines). The values of the different rate constants at some selected internal energies are listed in Table S1 of the Supporting Information. The frequencies and threshold energies used to compute these rate constants can be also found in the Supporting Information.

Knowing the internal vibrational energy distribution, it is possible to perform a kinetic analysis by means of the RRKM rate constants. In order to do so, we selected an upper value for the internal energy (vertical blue line in Figure 9, panels b and c) from the vibrational energy distributions corresponding to the maximum collision energy used in the experiments (84 and 65 kcal mol^{-1} for Ca and Sr, respectively in terms of internal energy). It can easily be seen that for these internal energies, all reactive channels but the latest (k_{15}) starting from min**1** are open in the case of $[Ca(formamide)]^{2+}$, whereas only the first two channels are open (k_{01} and k_{12}) when M = Sr. Thus, the difference between the two systems is mainly due to the

dx.doi.org/10.1021/jp5076059 | J. Phys. Chem. A 2014, 118, 10882−10893

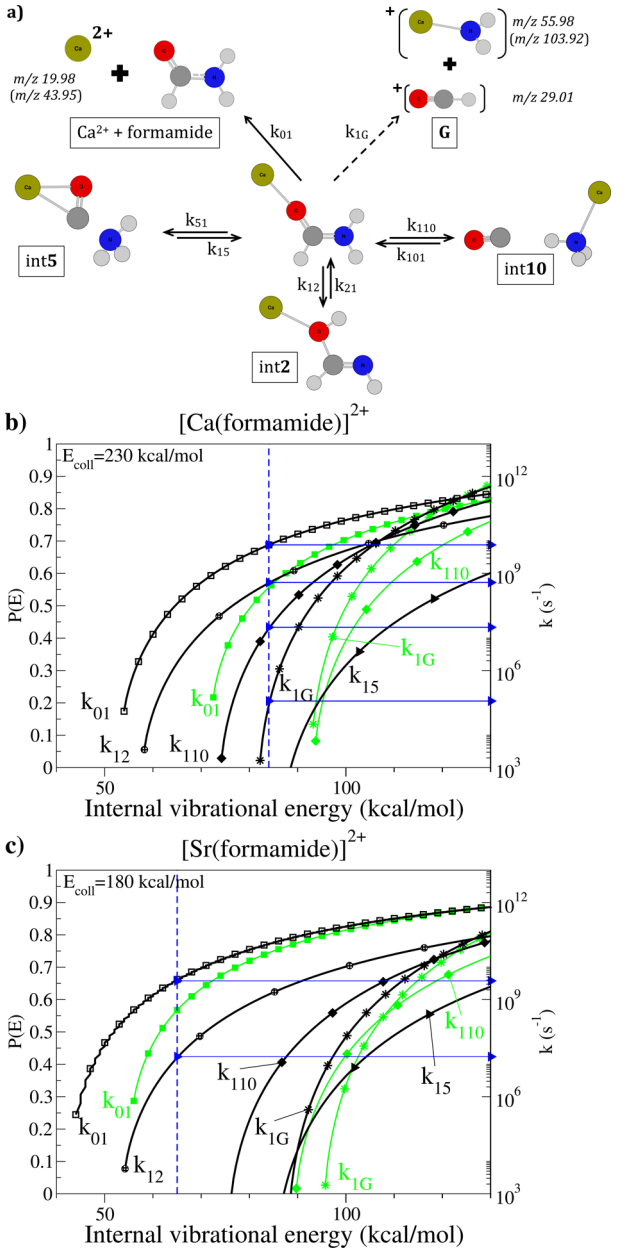

Figure 9. (a) Kinetic scheme for the reactions that can take place starting from min**1** for both $[Ca(formamide)]^{2+}$ and $[Sr(formamide)]^{2+}$. m/z ratios in parentheses are for M = Sr. In the bottom, RRKM rate constants corresponding to the aforementioned kinetic schemes (black lines). Rate constants taking into account rotational energy (27 and 18 kcal mol^{-1} for Ca and Sr, respectively) are also shown (green curves) when relevant (see text). Dash blue lines indicate the upper value for the internal energy.

difference in the internal vibrational energy distributions after collisional activation, given that the kinetic schemes for both metals are quite similar. Figure 9 also shows that in the case of $[Ca(formamide)]^{2+}$ for an internal energy of 84 kcal mol^{-1} (vertical blue line), the fastest reaction (in the order of hundreds of ps) is the one leading to formamide neutral loss yielding Ca^{2+} followed by the ones leading to int**2** (in the tens of nanoseconds time scale) and to int**10** (in the nanoseconds timescale). Finally, the **G** Coulomb explosion takes place in the microsecond time scale, 4 orders of magnitude slower than the formamide neutral loss. Note that even the fastest reaction obtained by RRKM analysis (i.e., hundreds of ps) does not happen in the time-span covered by the direct dynamics simulations (<2.5 ps), showing that a complete IVR mechanism, as assumed in RRKM theory, is not observed during the simulations.

Finally, it is worth noting that rotational excitation may play also an important role in the dynamics of these systems, especially when the moments of inertia of the TS are significantly different from those of the reactant. This is the case of the min**1** to formamide neutral loss, **G** products, and int**10** reactions. Hence, the effect on the RRKM rate constant k_{01}, k_{1G}, and k_{110} of adding 27 and 18 kcal mol^{-1} of rotational energy for Ca and Sr, respectively, is illustrated in Figure 9, panels b and c (green curves) (see section 2.2 for details on how rotational effects are taken into account in RKKM theory). It is apparent that for both metal ions, all the rate constants decrease and the curves appear shifted to higher energies, this shifting being different depending on the process. As a consequence, for M = Ca, the Coulomb explosion, k_{1G}, and the isomerization to yield int**10**, k_{110}, channels are closed, whereas k_{01} and k_{12} channels become competitive at the energy considered (blue line). For M = Sr, the effects are less dramatic because, although k_{01} is also shifted to higher energies, it does not cross k_{12} (i.e., it remains faster than k_{12}), and the other reactions do not take place for the energy considered.

This multitimescale approach can also be applied to investigate the evolution of the intermediates that can be reached from min**1**. This will be illustrated, as suitable examples, for int**2** and int**10** (see Scheme 1). The RRKM rate constants corresponding to these kinetic schemes are shown in Figures S10 and S11 of the Supporting Information.

Gathering together the results from chemical dynamics with results from RRKM coupled with energy transfer, we have seen that M^{2+} ions are obtained from both fast direct fragmentation mechanism and slow IVR statistical mechanisms. Following statistical mechanisms, the two systems will also form **A**, Coulomb explosion products: $[MOH]^+ + [HCNH]^+$, and **D**, neutral loss product: $[M(H_2O)]^{2+}$. However, formation of **D** will be dominant with respect to the formation of **A** for M = Sr, while the opposite is true for M = Ca, in agreement with the experimental evidence. For M = Ca, in which the vibrational excitation of the ions is higher, two more reaction channels are open, **B**: $[Ca(NH_3)]^{2+}$ and **G**: $[Ca(NH_2)]^+ + [HCO]^+$, which are however not accessible when M = Sr, again in agreement with the experimental observations. Therefore, the unassigned peak at m/z 52.46 in the [formamide-Sr]$^{2+}$ mass spectra should correspond to $[^{87}Sr(H_2O)]^{2+}$ rather than to $[Sr(NH_3)]^{2+}$, contrary to what we have previously suggested based on static calculations only.[57]

4. CONCLUDING REMARKS

The fragmentation of $[formamide\text{-}M]^{2+}$ complexes follows both statistical and dynamically driven mechanisms. Indeed, almost half of the trajectories reacts in a short timescale following a dynamical mechanism. The time to form the different products varies in a wide range, from few femtoseconds to nanoseconds. In the short timescale (<2.5 ps), we observed mainly dynamically driven reactions (impulsive collision mechanisms for energy transfer leading to a direct fragmentation mechanism), as formamide neutral loss. Coupling the internal vibrational energy distributions obtained from chemical dynamics simulations with RRKM rate constants, we could explore phenomena occurring at longer timescales. Thus, we

dx.doi.org/10.1021/jp5076059 | J. Phys. Chem. A 2014, 118, 10882−10893

could also account for "slow" reactions occurring via IVR mechanisms and leading to a wider range of products.

The use of direct dynamical simulations allowed us to explain the presence of the M^{2+} peak, otherwise impossible to explain based on PES analyses only (i.e., corresponding to the most endothermic exit channel). Furthermore, the dissimilarities between the two molecular ions such as the larger reactivity of the $[Ca(formamide)]^{2+}$ system or the absence of **G** Coulomb explosion in $[Sr(formamide)]^{2+}$ fragmentations, that cannot be explained neither from the PES topology nor using RRKM theory, can also be accounted for only when using the dynamical formalism. Therefore, by combining the three approaches, CID dynamics simulations, static (PES), and statistical (RRKM) analysis, we could explore a wide range of reaction timescales and ultimately account for all the products observed in the CID experimental spectra of $[Ca(formamide)]^{2+}$ and $[Sr(formamide)]^{2+}$ doubly charged cations, as well as explain the differences observed between these two ions.

■ ASSOCIATED CONTENT

Supporting Information

Potential energy curve, reaction time versus energy transfer graphs, selected distances for a trajectory, probability graphs, vibrational and rotational energy distributions, scattering plots, kinetic analysis, values of the RRKM rate constants, kinetic schemes, rate constant figures, and movies of reactions. This material is available free of charge via the Internet at http://pubs.acs.org.

■ AUTHOR INFORMATION

Corresponding Authors

*E-mail: manuel.yanez@uam.es.

*E-mail: riccardo.spezia@univ-evry.fr.

Notes

The authors declare no competing financial interest.

■ ACKNOWLEDGMENTS

This work has been partially supported by the DGI Project CTQ2012-35513-C02-01, by the COST Action CM1204, by the Project MADRISOLAR2, ref.: S2009PPQ/1533 of the Comunidad Autónoma de Madrid. A.M.S. acknowledges a FPI contract from the Ministerio de Economía y Competitividad of Spain. Computing time at Centro de Computación Científica of the Universidad Autónoma de Madrid is also acknowledged. This work was granted access to the HPC resources under the allocations x2013082123 and x2014082484 made by GENCI (Grand Equipement National de Calcul Intensif).

■ REFERENCES

(1) Laskin, J.; Futrell, J. H. Collisional activation of peptide ions in FT-ICR mass spectrometry. *Mass Spectrom. Rev.* **2003**, *22*, 158−181.

(2) Sleno, L.; Volmer, D. A. Ion activation methods for tandem mass spectrometry. *J. Mass Spectrom.* **2004**, *39*, 1091−1112.

(3) Mayer, P. M.; Poon, C. The mechanisms of collisional activation of ions in mass spectrometry. *Mass Spectrom. Rev.* **2009**, *28*, 608−639.

(4) Palumbo, A. M.; Smith, S. A.; Kalcic, C. L.; Dantus, M.; Stemmer, P. M.; Reid, G. E. Tandem mass spectrometry strategies for phosphoproteome analysis. *Mass Spectrom. Rev.* **2011**, *30*, 600−625.

(5) An, H. J.; Lebrilla, C. B. Structure elucidation of native N- and O-linked glycans by tandem mass spectrometry (tutorial). *Mass Spectrom. Rev.* **2011**, *30*, 560−578.

(6) Banoub, J. H.; El Aneed, A.; Cohen, A. M.; Joly, N. Structural investigation of bacterial lipopolysaccharides by mass spectrometry and tandem mass spectrometry. *Mass Spectrom. Rev.* **2010**, *29*, 606−650.

(7) Polfer, N. C.; Oomens, J. Vibrational spectroscopy of bare and solvated ionic complexes of biological relevance. *Mass Spectrom. Rev.* **2009**, *28*, 468−494.

(8) Harrison, A. G. To b or not to b: The ongoing saga of peptide b ions. *Mass Spectrom. Rev.* **2009**, *28*, 640−654.

(9) Shukla, A. K.; Futrell, J. H. Tandem mass spectrometry: Dissociation of ions by collisional activation. *J. Mass Spectrom.* **2000**, *35*, 1069−1090.

(10) McLuckey, S. A. Principles of collisional activation in analytical mass-spectrometry. *J. Am. Soc. Mass. Spectrom.* **1992**, *3*, 599−614.

(11) Wigner, E. The transition state method. *Trans. Faraday Soc.* **1938**, *34*, 29−41.

(12) Bunker, D. L. *Theory of Elementary Gas Reaction Rates*; Pergamon: Oxford, 1966.

(13) Robinson, P. J.; Holbrook, K. A. *Unimolecular Reactions*; Wiley: New York, 1972.

(14) Forst, W. *Theory of Unimolecular Reactions*; Academic: New York, 1973.

(15) Baer, T.; Hase, W. L.: *Unimolecular Reaction Dynamics. Theory and Experiments*; Oxford University Press: New York, 1996.

(16) Truhlar, D. G.; Garrett, B. C.; Klippenstein, S. J. Current status of transition-state theory. *J. Phys. Chem.* **1996**, *100*, 12771−12800.

(17) Forst, W. *Unimolecular Reactions*; Cambridge University Press: Cambridge, 2003.

(18) Henriksen, N. E.; Hansen, F. Y. *Theories of Molecular Reaction Dynamics: The Microscopic Foundation of Chemical Kinetics*; Oxford University Press: New York, 2008.

(19) Baercor, T.; Mayerfn, P. Statistical Rice-Ramsperger-Kassel-Marcus quasiequilibrium theory calculations in mass spectrometry. *J. Am. Soc. Mass. Spectrom.* **1997**, *8*, 103−115.

(20) Zimnicka, M.; Chung, T. W.; Moss, C. L.; Turecek, F. Perturbing Peptide Cation-Radical Electronic States by Thioxoamide Groups: Formation, Dissociations, and Energetics of Thioxopeptide Cation-Radicals. *J. Phys. Chem. A* **2013**, *117*, 1265−1275.

(21) Ichou, F.; Lesage, D.; Machuron-Mandard, X.; Junot, C.; Cole, R. B.; Tabet, J. C. Collision cell pressure effect on CID spectra pattern using triple quadrupole instruments: A RRKM modeling. *J. Mass Spectrom.* **2013**, *48*, 179−186.

(22) Ichou, F.; Schwarzenberg, A.; Lesage, D.; Alves, S.; Junot, C.; Machuron-Mandard, X.; Tabet, J.-C. Comparison of the activation time effects and the internal energy distributions for the CID, PQD and HCD excitation modes. *J. Mass Spectrom.* **2014**, *49*, 498−508.

(23) Kuki, A.; Nagy, L.; Szabo, K. E.; Antal, B.; Zsuga, M.; Keki, S. Activation energies of fragmentations of disaccharides by tandem mass spectrometry. *J. Am. Soc. Mass. Spectrom.* **2014**, *25*, 439−443.

(24) Fenn, P. T.; Chen, Y.-J.; Stimson, S.; Ng, C. Y. Dissociation of CH_3SH^+ by collisional activation: Evidence of non-statistical behaviour. *J. Phys. Chem. A* **1997**, *101*, 6513−6522.

(25) Chen, Y.-J.; Fenn, P. T.; Lau, K.-C.; Ng, C. Y.; Law, C.-K.; Li, W.-K. Study of the dissociation of $CH_3SCH_3^+$ by collisional activation: Evidence of non-statistical behaviour. *J. Phys. Chem. A* **2002**, *106*, 9729−9736.

(26) Liu, J.; Song, K.; Hase, W. L.; Anderson, S. L. Direct dynamics study of energy transfer and collision-induced dissociation: Effects of impact energy, geometry, and reactant vibrational mode in H_2CO^+-Ne collisions. *J. Chem. Phys.* **2003**, *119*, 3040−3050.

(27) Martínez-Núñez, E.; Vázquez, S. A.; Marqués, J. M. C. Quasiclassical trajectory study of the collision-induced dissociation of CH_3SH^+ + Ar. *J. Chem. Phys.* **2004**, *121*, 2571−2577.

(28) Martínez-Núñez, E.; Fernández-Ramos, A.; Vázquez, S. A.; Marqués, J. M. C.; Xue, M.; Hase, W. L. Quasiclassical dynamics simulation of the collision-induced dissociation fo $Cr(CO)_6^+$ with Xe. *J. Chem. Phys.* **2005**, *123*, 154311.

(29) Martínez-Núñez, E.; Vázquez, S. A.; Aoiz, F. J.; Castillo, J. F. Quasiclassical trajectory study of the collision-induced dissociation

dynamics of Ar + CH_3SH^+ using an ab initio interpolated potential energy surface. *J. Phys. Chem. A* **2006**, *110*, 1225−1231.
(30) Spezia, R.; Cimas, Á.; Gaigeot, M.-P.; Salpin, J.-Y.; Song, K.; Hase, W. L. Collision induced dissociation of doubly-charged ions: Coulomb explosions vs. neutral loss in $[Ca(urea)]^{2+}$ gas phase unimolecular reactivity via chemical dynamics simulations. *Phys. Chem. Chem. Phys.* **2012**, *14*, 11724−11736.
(31) Meroueh, S. O.; Wang, Y.; Hase, W. L. Direct dynamics simulations of collision- and surface-induced dissociation of N-protonated glycine. Shattering fragmentation. *J. Phys. Chem. A* **2002**, *106*, 9983−9992.
(32) Lourderaj, U.; Hase, W. L. Theoretical and computational studies of non-RRKM unimolecular dynamics. *J. Phys. Chem. A* **2009**, *113*, 2236−2253.
(33) Hendell, E.; Even, U.; Raz, T.; Levine, R. D. Shattering of clusters upon surface impact: An experimental and theoretical study. *Phys. Rev. Lett.* **1995**, *75*, 2670−2673.
(34) Raz, T.; Levine, R. D. On the shattering of clusters by surface impact heating. *J. Chem. Phys.* **1996**, *105*, 8097.
(35) Schultz, D. G.; Hanley, L. Shattering of $SiMe_3^+$ during surface-induced dissociation. *J. Chem. Phys.* **1998**, *109*, 10976.
(36) Burroughs, J. A.; Wainhaus, S. B.; Hanley, L. Impulsive excitation of $FeCp_2^+$ and $SiMe_3^+$ during surface-induced dissociation at organic multilayers. *J. Chem. Phys.* **1995**, *103*, 6706.
(37) Meroueh, O.; Hase, W. L. Effect of surface stiffness on the efficiency of surface-induced dissociation. *Phys. Chem. Chem. Phys.* **2001**, *3*, 2306.
(38) Meroueh, O.; Song, K.; Hase, W. L. Dynamics of $Cr(CO)_6^+$ collisions with hydrogenated surfaces. *J. Chem. Phys.* **2003**, *118*, 2893.
(39) Wang, Y.; Hase, W. L.; Song, K. Direct dynamics stufy of N-protonated diglycine surface-induced dissociation. Influence of collision energy. *J. Am. Soc. Mass Spectrom.* **2003**, *14*, 1402.
(40) Nordholm, S.; Schranz, H. W.; Freasier, B. C.; Hamer, N. D. Diatomic dissociation rate theory. I. Angular momentum conservation and impulsive collisions in the low pressure limit. *Chem. Phys.* **1989**, *129*, 351−361.
(41) In some works,[31,67] the term "shattering" is also used in the context of CID, but when the same term is used in the SID, this does not imply a nonstatistical mechanism.[33,34]
(42) Schöder, D.; Schwarz, H. Generation, stability, and reactivity of small, multiply charged ions in the gas phase. *J. Phys. Chem. A* **1999**, *103*, 7385−7394.
(43) Heller, D. N.; Yergey, J.; Cotter, R. J. Doubly-charged ions in desorption mass spectrometry. *Anal. Chem.* **1983**, *55*, 1310−1313.
(44) Katritzky, A. R.; Shipkova, P. A.; Burton, R. D.; Allin, S. M.; Watson, C. H.; Eyler, J. R. Investigation of doubly charged organic cations by electrospray ion cyclotron resonance mass spectrometry. *J. Mass Spectrom.* **1995**, *30*, 1581−1587.
(45) Miller, J. M.; Balasanmugam, K.; Nye, J.; Deacon, G. B.; Thomas, N. C. Observation of doubly charged ions in fast atom bombardment mass spectrometry: Ruthenium(II) complexes in a nitrobenzyl alcohol matrix. *Inorg. Chem.* **1987**, *26*, 560−562.
(46) Price, S. D. Interactions of molecular doubly charged ions with atoms, molecules and photons. *J. Chem. Soc., Faraday Trans.* **1997**, *93*, 2451−2460.
(47) Roth, L. M.; Freiser, B. S. Gas-phase chemistry and photochemistry of doubly charged transition-metal-containing ions. *Mass Spectrom. Rev.* **1991**, *10*, 303−328.
(48) Breig, E. L.; Torr, M. R.; Torr, D. G.; Hanson, W. B.; Hoffman, J. H.; Walker, J. C. G.; Nier, A. O. Doubly charged atomic oxygen ions in the thermosphere, 1. Photochemistry. *J. Geophys. Res.* **1977**, *82*, 1008−1012.
(49) Simon, C.; Lilensten, K.; Dutuit, O.; Thissen, R.; Witasse, O.; Alcaraz, C.; Soldi-Lose, H. Prediction and modelling of doubly-charged ions in the Earth's upper atmosphere. *Ann. Geophys.* **2005**, *23*, 781−797.
(50) Thissen, R.; Witasse, O.; Dutuit, O.; Wedlund, C. S.; Gronoffe, G.; Lilensten, J. Doubly-charged ions in the planetary ionospheres: A review. *Phys. Chem. Chem. Phys.* **2011**, *13*, 18264−18287.
(51) Victor, G. A.; Constantinides, E. R. Double photoionization and doubly charged ions in the thermosphere. *Geophys. Res. Lett.* **1979**, *6*, 519−522.
(52) Arrhenius, G. O. Crystals and life. *Helv. Chim. Acta* **2003**, *86*, 1569−1586.
(53) Franchi, M.; Ferris, J. P.; Gallori, E. Cations as mediators of the adsorption of nucleic acids on clay surfaces in prebiotic environments. *Origins Life Evol. Biospheres* **2003**, *33*, 1−16.
(54) Julian, R. R.; Beauchamp, J. L. Abiotic synthesis of ATP from AMP in the gas phase: Implications for the origin of biologically important molecules from small molecular clusters. *Int. J. Mass Spectrom.* **2003**, *277*, 147−159.
(55) Lathe, R. Fast tidal cycling and the origin of life. *Icarus* **2003**, *168*, 18−22.
(56) Morowitz, H. J.; Srinivasan, V.; Smith, E. Ligand field theory and the origin of life as an emergent feature of the periodic table of elements. *Biol. Bull.* **2010**, *219*, 1−6.
(57) Martín-Sómer, A.; Gaigeot, M.-P.; Yanez, M.; Spezia, R. A RRKM study and a DFT assessment on gas-phase fragmentation of formamide-M^{2+} (M = Ca, Sr). *Phys. Chem. Chem. Phys.* **2014**, *16*, 14813−14825.
(58) Eizaguirre, A.; Mó, O.; Yáñez, M.; Salpin, J.-Y. Modeling the interactions between peptide functions and Sr^{2+}: Formamide-Sr^{2+} reactions in the gas phase. *Phys. Chem. Chem. Phys.* **2011**, *13*, 18409−18417.
(59) Eizaguirre, A.; Mó, O.; Yáñez, M.; Salpin, J.-Y.; Tortajada, J. Modelling peptide-metal dication interactions: Formamide-Ca^{2+} reactions in the gas phase. *Org. Biomol. Chem.* **2012**, *10*, 7552−7561.
(60) Meroueh, O.; Hase, W. L. Collisional activation of small peptides. *J. Phys. Chem. A* **1999**, *103*, 3981−3990.
(61) Kaupp, M.; Schleyer, P. R.; Stoll, H.; Preuss, H. Pseudopotential approaches to Ca, Sr and Ba hydrides. Why are some alkaline earth MX_2 compounds bent? *J. Chem. Phys.* **1991**, *94*, 1360−1366.
(62) Boys, S. F.; Bernardi, F. The calculation of small molecular interactions by the differences of separate total energies. Some procedures with reduced errors. *Mol. Phys.* **1970**, *19*, 553−556.
(63) Lee, C.; Yang, W.; Parr, R. G. Development of the Colle-Salvetti correlation-energy formula into a functional of the electron density. *Phys. Rev. B* **1988**, *37*, 785−789.
(64) Gill, P. M. W. A new gradient-corrected exchange functional. *Mol. Phys.* **1996**, *89*, 433−445.
(65) Becke, A. D. Density-functional exchange-energy approximation with correct asymptotic behavior. *Phys. Rev. A* **1988**, *38*, 3098−3100.
(66) Meroueh, O.; Hase, W. L. Energy transfer pathways in the collisional activation of peptides. *Int. J. Mass Spectrom.* **2000**, *201*, 233−244.
(67) Spezia, R.; Salpin, J.-Y.; Gaigeot, M.-P.; Hase, W. L.; Song, K. Protonated urea collision-induced dissociation. Comparison of experiments and chemical dynamics simulations. *J. Phys. Chem. A* **2009**, *113*, 13853−13862.
(68) Jeanvoine, Y.; Gaigeot, M. P.; Hase, W. L.; Song, K.; Spezia, R. Collision induced dissociation of protonated urea with N_2: Effects of rotational energy on reactivity and energy transfer via chemical dynamics simulations. *Int. J. Mass Spectrom.* **2011**, *308*, 289−298.
(69) Hu, X.; Hase, W. L.; Pirraglia, T. Vectorization of the general Monte Carlo classical trajectory program VENUS. *J. Comput. Chem.* **1991**, *12*, 1014−1024.
(70) Hase, W. L.; Duchovic, R. J.; Hu, X.; Komornicki, A.; Lim, K. F.; Lu, D.-H.; Peslherbe, G. H.; Swamy, K. N.; Linde, S. R. V.; Varandas, A.; Wang, H.; Wolf, R. J. *QCPE* **1996**, *16*, 671.
(71) Douglas, D. J. Applications of collision dynamics in quadrupole mass spectrometry. *J. Am. Soc. Mass. Spectrom.* **1998**, *9*, 101−113.
(72) Frisch, M. J.; Trucks, G. W.; Schlegel, H. B.; Scuseria, G. E.; Robb, M. A.; Cheeseman, J. R.; Scalmani, G.; Barone, V.; Mennucci, B.; Petersson, G. A.; et al.*Gaussian09*, revision C.01; Gaussian, Inc.: Wallingford, CT, 2010.
(73) Swope, W. C.; Andersen, H. C.; Berens, P. H.; Wilson, K. R. A computer simulation method for the calculation of equilibrium

constants for the formation of physical clusters of molecules: Application to small water clusters. *J. Chem. Phys.* **1982**, *76*, 637−649.
(74) Paranjothy, M.; Sun, R.; Zhuang, Y.; Hase, W. L. Direct chemical dynamics simulations: Coupling of classical and quasiclassical trajectories with electronic structure theory. *Comput. Mol. Sci.* **2013**, *3*, 296−316.
(75) Glendening, E. D.; Badenhoop, J. K.; Reed, A. E.; Carpenter, J. E.; Bohman, J. A.; Morales, C. M.; Weinhold, F. *NBO 5.0*; Theoretical Chemistry Institute, University of Wisconsin: Madison, 2001.
(76) Zhu, L.; Hase, W. L. Comparison of models for calculating the RRKM unimolecular rate constant k(E,J). *Chem. Phys. Lett.* **1990**, *175*, 117−124.
(77) Townes, C. H.; Schadow, A. L. *Microwave Spectrometry*; McGraw-Hill: New York, 1955.
(78) Rodgers, M. T.; Armentrout, P. B. Statistical modeling of competitive threshold collision-induced dissociation. *J. Chem. Phys.* **1998**, *109*, 1787.
(79) Turi, V. D.; Ervin, K. M. Competitive threshold collision-induced dissociation: gas-phase acidities and bond dissociation energies for a series of alcohols. *J. Phys. Chem. A* **1999**, *103*, 6911.
(80) Armentrout, P. B.; Ervin, K. M.; Rodgers, M. T. Statistical rate theory and kinetic energy-resolved ion chemistry: Theory and applications. *J. Phys. Chem. A* **2008**, *112*, 10071−10085.
(81) Rodgers, M. T.; Ervin, K. M.; Armentrout, P. B. Statistical modeling of collision-induced dissociation thresholds. *J. Chem. Phys.* **2008**, *106*, 4499.
(82) de Sainte Claire, P.; Peslherbe, G. H.; Hase, W. L. Energy transfer dynamics in collision-induced dissociation of Al_6 and Al_{13} clusters. *J. Phys. Chem.* **1995**, *99*, 8147−8161.